ENVIRONMENTAL CHAMBER WALL LOSS CHARACTERIZATION

By

Shunhua Lin

A capstone project submitted for
Graduation with University Honors

December 10, 2016

University Honors
University of California, Riverside

APPROVED

_____
Dr. David Cocker
Department of Chemical and Environmental Engineering

_____
Dr. Richard Cardullo, Howard H Hays Chair and Faculty Director, University Honors
Associate Vice Provost, Undergraduate Education

ABSTRACT

Understanding the mechanism of secondary organic aerosols (SOA) formation is one of the keys to control air pollution. This process was started by testing SOA formation in an environmental chamber at the laboratory. However, former studies indicated that SOA formation might be underestimated due to the deposition of SOA on the chamber walls. Reexamining previous studies in this area can reveal more about the mechanism of SOA formation, helping to find better solutions for air pollution control. In this work, the selected former studies in SOA formation were reanalyzed. In particular, 100 sets of data generated from the laboratory at the University of California, Riverside (UCR) about SOA formation were reexamined and conclusions were made accordingly. First, the walls of the environmental chamber at the laboratory was one of the factors resulting in the underestimation of SOA formation. Second, the chemical and physical properties of the reactants had effects on the SOA formation. Decreasing the molecular weight (MW) and size of the reactant(s) increased the effect of SOA formation. Isomers of a compound had diverse contributions on the SOA formation due to the different positions of their functional group(s). Third, different compositions of the reactants in a system had various outcomes on the SOA formation. For the same components in a system, increasing the concentration of some of the reactant(s) increased the SOA formation. Finally, no functional relationships between the wall loss rate (β) and any one of the parameters (PM(num), M_o, T, and MW), the non-carbon species (NO, H_2O_2, O_3, and N_2O_5), the number of starting carbon in aromatic species from C6 to C9, and the chamber's volume (or surface area), were detected in the data under study. Future study is recommended to focus more on this area. In addition, the effect of extremely low volatile organic compounds (ELVOCs) on SOA

formation and the effects of different chamber wall materials on wall-loss and SOA formation are recommended for future study.

Acknowledgements

This work was instructed and guided by Dr. David Cocker, a professor at the Chemical and Environmental Engineering Department at the University of California, Riverside. His guidance was highly valued and the author of this paper is grateful for his mentoring. The concept of this work was inspired step by step by the efforts of the faculty members, especially the Honors director, Dr. Richard Cardullo, my current and former Honors advisors, Aaron Bushong, Mayra Jones, and Jane Elizabeth Kim, at the University Honors Department at UCR. Their inspiration and encouragement are appreciated. Also, I wish to acknowledge the graduate student, Paul Van Rooy's helps in the explanation about the experimental data from the UCR laboratory. His explanations were the key to understand and further initiate the process of the analysis about the data. I am also thankful for all the authors of the selected studies in this work.

TABLE OF CONTENTS

Lists of Tables and Figures

Introduction

Aerosol is a system composed of solid or liquid particles in a range of 10^{-9} m to 10^{-4} m suspended in a gaseous medium (Kulkarni et al., 2011). There are two types of aerosols, primary and secondary aerosols. Primary aerosols are aerosols introduced directly from a source into the atmosphere. Examples are volcanic dust and soot. Secondary aerosols are aerosols generated in situ aggregation or nucleation from gas phase molecules. Examples are sulfates (SO_4^{2-}) from sulfur dioxide (SO_2) and nitrates (NO_3^-) from NO_x, a mixture of nitric oxide (NO) and nitrogen dioxide (NO_2). Atmospheric aerosols are mainly composed of organic materials. Most of the organic materials condense to the particle phase from the gas phase and are called Secondary Organic Aerosols (SOA) (Goldstein, Allen H., and John H. Seinfeld, 2015). Aerosols are responsible for the phenomena of air pollution such as dust, smog, and suspended particulate matter (PM). Understanding the SOA formation mechanism is the starting point for air pollution control. This understanding can be achieved by conducting an experiment in a laboratory using an environmental chamber. However, previous studies have indicated that the SOA formation might be underestimated due to the loss of SOA to the walls of the chamber. Reexamining the wall loss characterization in the environmental chamber can reveal more about the mechanism of SOA formation, helping to seek out better solutions for air pollution control. In this study, the general environmental chamber characterization was described; the experimental results from the selected former studies, especially the studies from the UCR CE-CERT laboratory about SOA formation, were reanalyzed; and conclusions were made accordingly.

Experimental Facilities

The experimental facilities consisted of an enclosure housing a chamber with devices for the conditions control, computer software for simulation, and reactants for the experiment. The details about the individual pieces of equipment are provided in the following section.

Environmental Chamber

The chamber in this study was from the UCR laboratory, a rectangular chamber made of fluorinated ethylene propylene (FEP) Teflon. Its flexible walls allowed samples to be taken out without replacement by collapsing inward, facilitated the contamination control process during sample withdrawing (Leskinen et al., 2015). The following diagram, figure 1. illustrates this chamber.

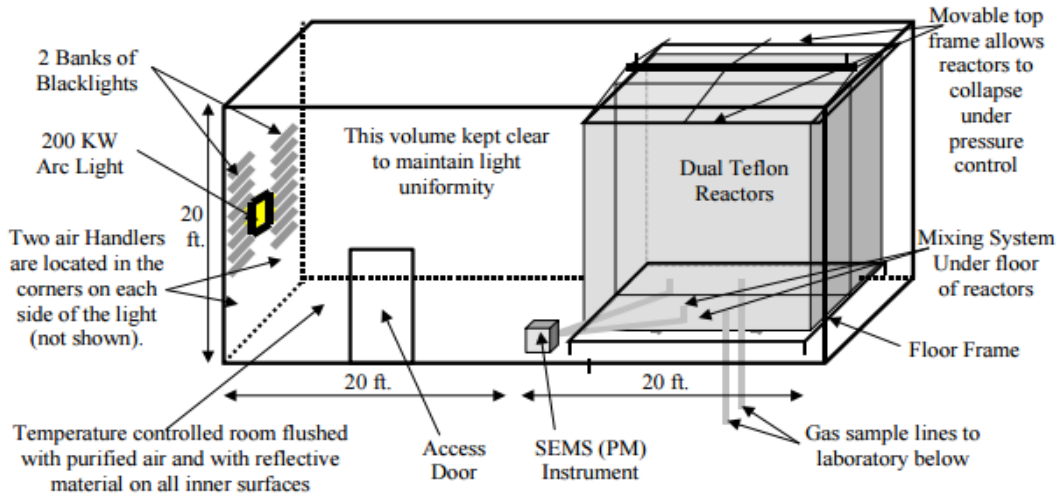

Figure 1. Schematic of the environmental chamber reactors and enclosure.

The chamber in Figure 1. was composed of two 85m^3 reactors (A side and B side reactors) located in a 453m^3 enclosure. The enclosure was continuously flushed with

purified air and its temperature was well controlled. Two light sources, a 200 KW arc lamp and banks of blacklights, were used alternatively to produce light in the UV and visible spectrums, similar to sunlight. Reflective aluminum panels were employed to cover the interior of the enclosure to maximize light intensity as well as maintain light uniformity. The pressure inside the chamber was maintained at a predefined, positive pressure and was continuously monitored by pressure sensors. When the reactors expanded or collapsed due to filling or emptying, motors controlled by pressure sensors raised or lowered the chamber's moveable top frame, which was held to the ceiling by cables connected to the motors. The duration of the experiment was determined by the volume of the reactors. When the volume of one of the reactors reached approximately 1/3 of the maximum value, the experiment was terminated (Carter et al., 2005).

Temperature Control and Its Homogeneity

During the experiment, the temperature in the chamber was continuously monitored by Teflon-coated fans coupled with Siemens QFFM2016 (Wang et al., 2014), or by calibrated thermocouples attached to thermocouple boards on a computer data acquisition system (Carter et al., 2012). Homogeneous temperature was maintained in the range of 296-307^{o}K, with deviation of ±1^{o}K.

Light Spectrum and Intensity

Irradiation over a predefined range of wavelength, for example, 300-850nm, produced by the black lamps was monitored by instruments such as EPP2000CXR-50 concave grating spectrometer, or LiCor LI-1800 spectroradiometer. The photolysis rate of NO_2 represented the light intensity, which was measured by a steady-state actinometry. By

continuously measuring the concentrations of NO, NO_2, and O_3 generated through irradiating NO_2 in feed, the photolysis rate of NO_2, J_{NO2} was computed according to the equation

$$J_{NO_2} = k_{NO+O_3}[NO][O_3]/[NO_2],$$

Where [NO], [O_3], and [NO_2] represented, respectively, the concentration of the species NO, O_3 and NO_2 in molecule/cm^3. K_{NO+O3} was the rate constant of ozone and NO reaction (Atkinson et al. 2004, Wang et al. 2014).

Mixing

The air in the enclosure was purified with no detectable particles (< 0.2 particles/cm^3), non-methane hydrocarbons (<1ppb), and NO_x (<10ppt). Inside a reactor, the fan was placed near the feeding line at the floor of the reactor for mixing the gaseous content. Ozone was used as a tracer to test the gas-phase mixing time. By injecting a particular amount of ozone into the reactor followed by analyzing its concentration in the reactor, the mixing time was determined (Wang et al., 2014).

Wall Loss of Gases

The wall loss rates of gaseous species were evaluated by continuously monitoring their decay in the dark after a predefined amount of these species were injected into the reactor chamber. Table 1. showed the wall loss rate of the gas species, NO, NO_2, and O_3, in different smog chambers provided by the previous study from Wang et al (Wang et al., 2014).

Table 1.

The wall loss rate of NO, NO_2, and O_3 in different smog chambers:

N/A =no data is available.

species	#run	T(k)	RH(%)	Rate(wall loss)×10^{-4}/min			
				GIG-CAS ($30m^3$)	ERT($60m^3$)	EUPHORE($200m^3$)	PSI($27m^3$)
O_3	4	296.7	<10	1.31±0.24	0.5-3	1.8	2.4
NO	9	296.7	<10	1.41±0.10	0-5.4	N/A	N/A
NO_2	4	296.7	<10	1.39±0.68	0-2	N/A	0.13-2.52

From this table, it was evident that the wall loss rate was inversely proportional to the molecular weight of the species. The decreasing order of the wall loss rate of these species were $\beta_{NO} > \beta_{NO2} > \beta_{O3}$ and that in the molecular weight of the species are $O_3 > NO_2 > NO$.

Particle Wall Loss

The particle wall loss rate depends on the particle size, the charged wall, and the turbulent diffusion as well as the molecular diffusion. It is proportional to the particle concentration. The relationship between the particle number and the weighted wall loss rate is expressed mathematically as

$$\frac{dN(d_p,t)}{dt} = -K_N(d_p)N(d_p,t),$$

$\ln[N_0(d_p, t) / N(d_p, t)] = K_N(d_p)\, t$

Where $N_0(d_p, t)$ is the initial particle number concentration, $N(d_p, t)$ is the particle number concentration at time t, d_p is the particle diameter, and $K_N(d_p)$ is the particle number loss coefficient. $K_N(d_p)$ can be estimated from the plot, particle number concentration vs. time, in the experiment when no new particle is generated. Table 2. showed the particle wall loss rates in different smog chambers quoted from a former experiment (Cocker et al., 2001a, Wang et al., 2014).

Table 2. Comparison of particle wall loss rates in different volumes of smog chambers

chamber	V(m^3)	Wall material	Rate(wall loss) #particles/h	Particle lifetime(h)	reference
GIG-CAS	30	FEP	0.17	5.9	Wang et al(2014)
PSI	27	FEP	0.21	4.8	Paulsen et al.(2005)
Caltech	28	FEP	0.20	5.0	Cocker et al(2001a)
UCR	90	FEP	0.29	3.4	Carter et al(2005)
EUPHORE	200	FEP	0.18	5.6	Martin-Reviejo and Wirtz(2005)
SAPHIR	270	FEP	0.27	3.7	Rollins et al(2009)
CMU	12	FEP	0.4	2.5	Donahue et al(2012)

From the table above, it was observed that with the smallest chamber volume (or greatest wall surface area), 12 m^3, the CMU chamber had the fastest particle wall loss rate, 0.4 particles/h. Whereas the EUPHORE chamber had the second slowest particle wall loss rate, 0.18 particles/h, with the second greatest chamber volume, 200 m^3.

SOA Yield

The SOA formation was evaluated by carrying out a series of experiments on α-pinene ozonolysis in the dark. The SOA yield, Y, was computed from the equation below:

$$Y = \frac{\Delta M_0}{\Delta \mathrm{ROG}},$$

where $\Delta\,\mathrm{ROG}$ was the mass concentration of reactive organic gas (ROG) after reaction, and M_0 was the total mass concentration of organic aerosols formed in μg/m^3. Y was also the function of M_o based on the following equation:

$$Y = M_0 \sum \left(\frac{\alpha_i K_{\mathrm{om},i}}{1 + K_{\mathrm{om},i} M_0}\right),$$

Where $K_{om,i}$ and α_i were, respectively, the mass-based absorption equilibrium partitioning coefficient and stoichiometric coefficient of the project, i. By plotting Y vs. M_o, the SOA yield at a particular M_o value was found on the graph (Wang et al., 2014). Figure 2. showed

a sample graph of Y vs. M_o from the two reactors, UCR and Caltech reactors, as well as a best-bit line for the data sets (Carter et al., 2005).

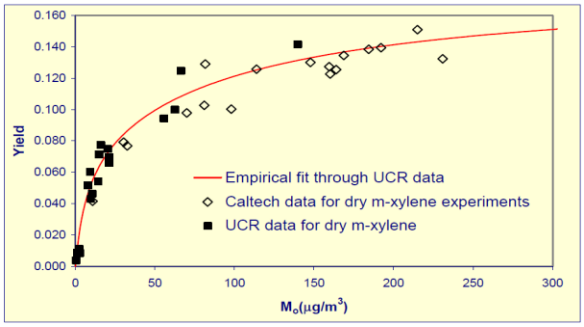

Figure 2. SOA yield vs M_0 for m-xylene/NO_x system from UCR and Caltech reactors as well as the best-fit for the two data set.

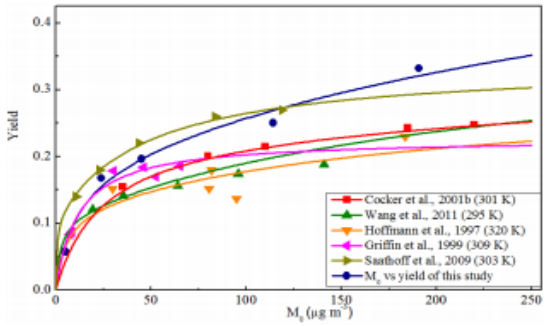

Figure 3. SOA yield of α-pinene ozonolysis from various reactors under dry condition. The blue line is the best-fit line for the data from GIG-CAS chamber, Wang et al.'s experiment.

Figure 2. showed that under the experimental conditions, the SOA yield increased rapidly below M_o=25μg/m^3. Above that value, the increase in SOA yield started to slow and approached a constant value. Similar results can be seen from Figure 3., the study conducted by Wang et al (Wang et al., 2014).

Reactants

The reactants and their compositions were various depending on the test objective. Usually, NO_x, O_3, toluene, and OH radical sources such as H_2O_2 were employed. Some experiments also used ammonium sulfate as seed particles or even use other reactants. For example, in the wood-smoke smog-chamber in Bian et al.'s experiment various types of substances, such a Wire Grass, Black Spruce, and Turkey Oak, were used as smoke sources (Bian et al., 2015).

Simulation Software

Various software models were used for the simulation of the experiment. The models used in the selected former studies were the Generator for Explicit Chemistry, the Kinetics

of the Organics in the Atmosphere modeling tool, the Master Chemical Mechanism, the TwO-Moment Aerosol Sectional, and the Statistical Oxidation Model.

Method of Experiment

The experiment was carried out in an indoor Teflon film chamber under UV-visible light conditions described above. The reactants were injected through Teflon injection lines located at the bottom of the chamber, separated from the sampling lines (Carter et al., 2012). After the reactants were injected, stabilized, and sampled, the irradiation process was started by turning on the blacklights (Carter et al., 2012). During the irradiation, the pressure in the enclosure was kept slightly greater than the pressure in the surrounding room to prevent outside air leaking inward, resulting in contamination. The pressure in the chamber was maintained at about 5 pascals greater than the pressure outside by lowering the top frames as needed. The temperature in the chamber was allowed to fluctuate within $2^{o}K$ during the experiments. Together with the relative humidity, the temperature of the chamber was measured with an electronic thermos-hygrometer. The particle data, such as the particle size distribution, was obtained by using a Scanning Mobility Particle Sizer coupled with a Condensation Nuclei Counter to analyze the sample in the chamber. It was assumed that the loss of aerosols to the chamber walls was a first order decay and the particle data from the wall-loss was corrected based on this assumption. An HP 5890 GC-FID was employed to measure the gas-phase toluene concentrations. The chamber was cleaned between runs by emptying the air inside the chamber and re-filling it with purified air at least six times while the lights were off. The experiment was terminated when the volume of the reactor was reduced to 1/3 of its maximum value. The setup of the experiment was positioned on the second floor of the laboratory, facilitated feeding reactants and withdrawing the sample from the bottom of the chamber (Carter et al., 2005).

Results

In this paper, 100 sets of data generated from the experiments conducted at the UCR laboratory using the chamber described at the "Environmental chamber" section and illustrated in Figure 1. were reanalyzed below. In these data sets, each experiment or run had its own run number defined as EPAXXXX. EPA stood for Environmental Protection Agency and XXXX was a four-digit code, defining the run. The symbol, β, represented the wall loss rate in particles/minute. PMVOLUCR was the uncorrected volume of PM in the chamber and PMVOLCOR represented the corrected one. Both parameters had a unit in $\mu g/cm^3$. PMNUMCOR or PM(num) was the corrected number of PM in the chamber in cm^{-3} and "t" was time in minutes. T was temperature in Kelvin, MW stood for molecular weight in g/mol. In the following analysis, the letters "EPA" in the run number was omitted for convenience. The data sets under study were from EPA1151 to EPA1253; however, only results from completed experiments with representative data were shown here. The data were analyzed and curves about β vs. PM(num), β vs. M_o, β vs. T, β vs. MW, β vs. species (NO, H_2O_2, N_2O_5), β vs. C's (C6-C9), PMVOLUCR vs. t, PMVOLCOR vs. t, and PMNUMCOR vs. t were generated. The resulted graphs, Figures (1) - (7), were shown in the following section and Figures (8)-(19) were displayed in the appendix.

Graphs.

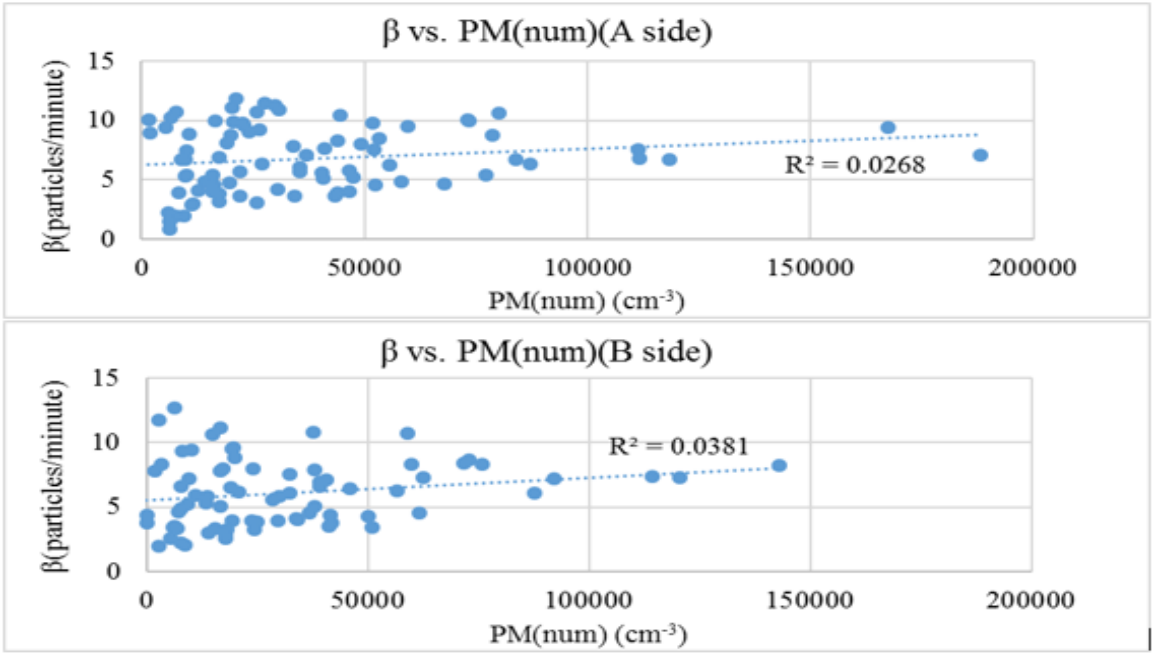

Figure (1). β vs. PM(num) from A side (top) and B side (bottom). The wall loss rate, β, shows no correlation with the PM number as it alters. R^2's from both sides of the reactors are less than 0.04.

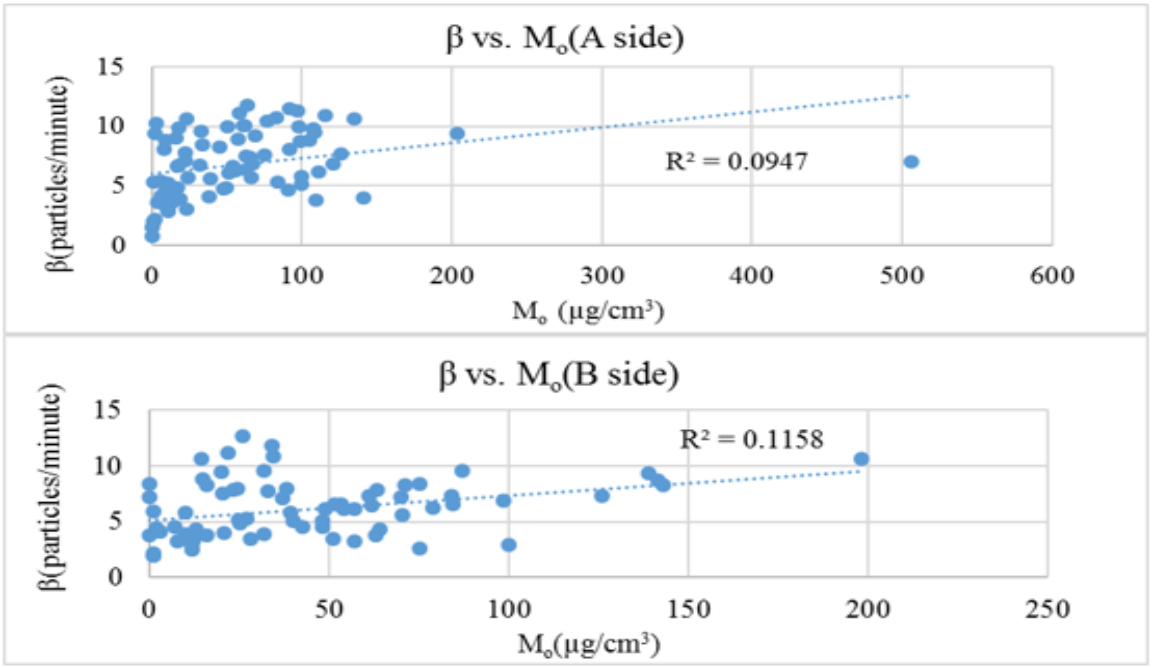

Figure (2). β vs. M_o from A side (top) and B side (bottom). With the R^2 less than 0.2, the wall loss rate, β, from either side of the chambers is independent from the total mass concentration of the organic aerosols formed in the chamber, M_o.

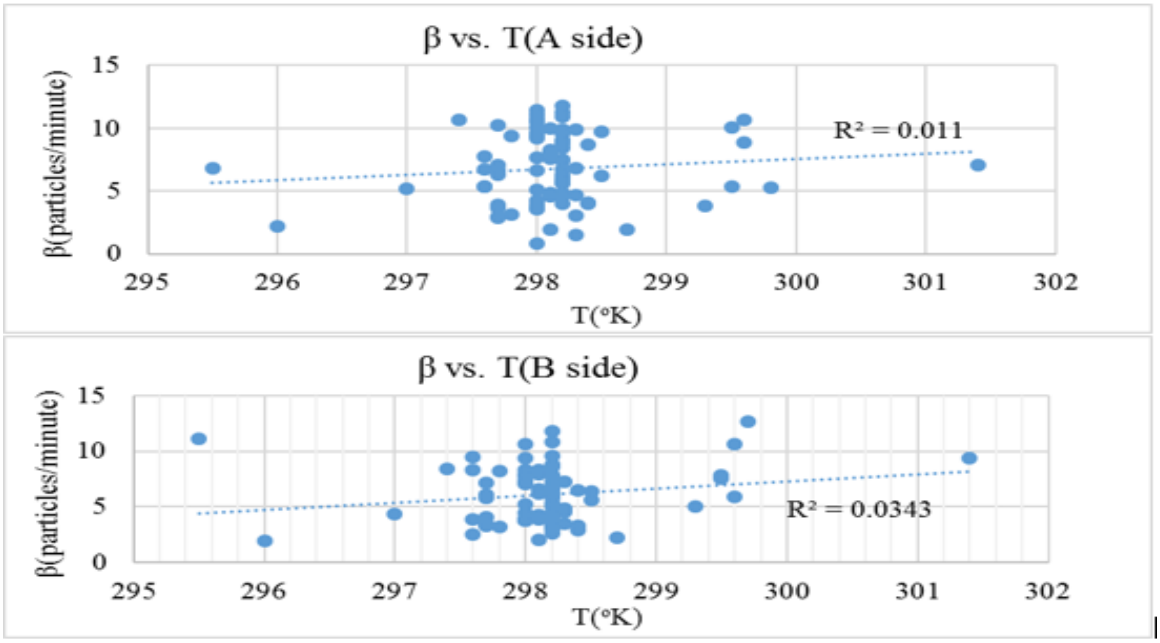

Figure (3). β vs. T(°K) from A side (top) and B side (bottom). The wall loss rate, β, changes independently as temperature, T, differs. R^2's from both sides of the reactors are less than 0.04.

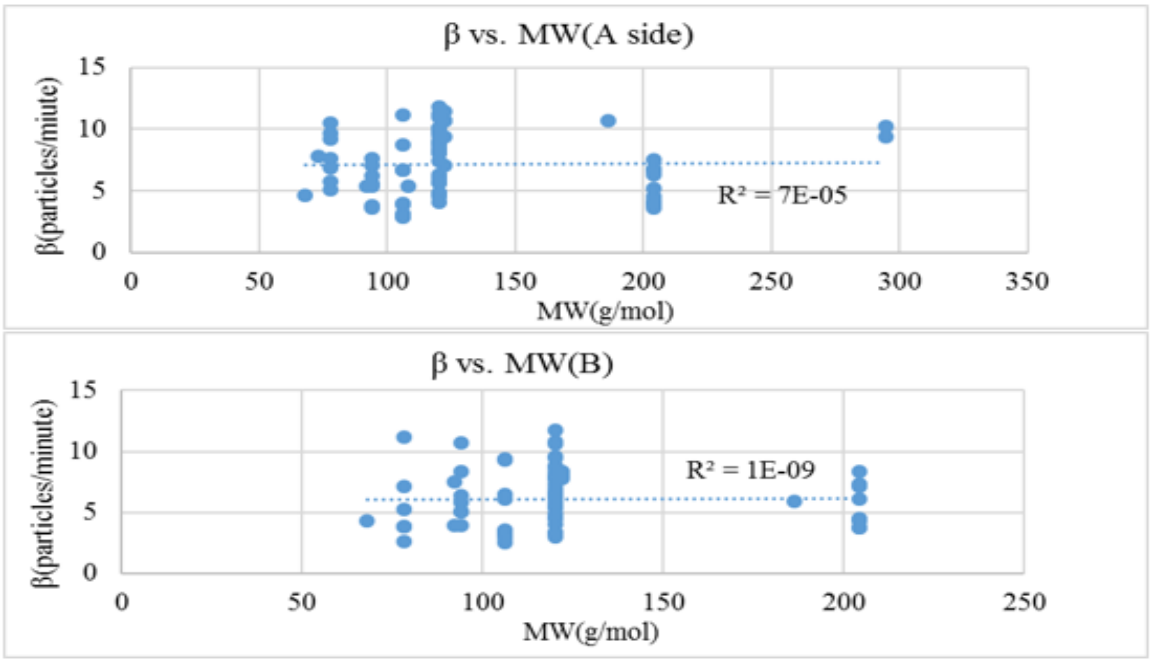

Figure (4). β vs. MW (molecular weight) from A side (top) and B side (bottom). With a significantly small R^2 value, less than $1*10^{-4}$, a functional relationship between the wall loss rate, β, and the molecular weight of compounds, MW, is not identified.

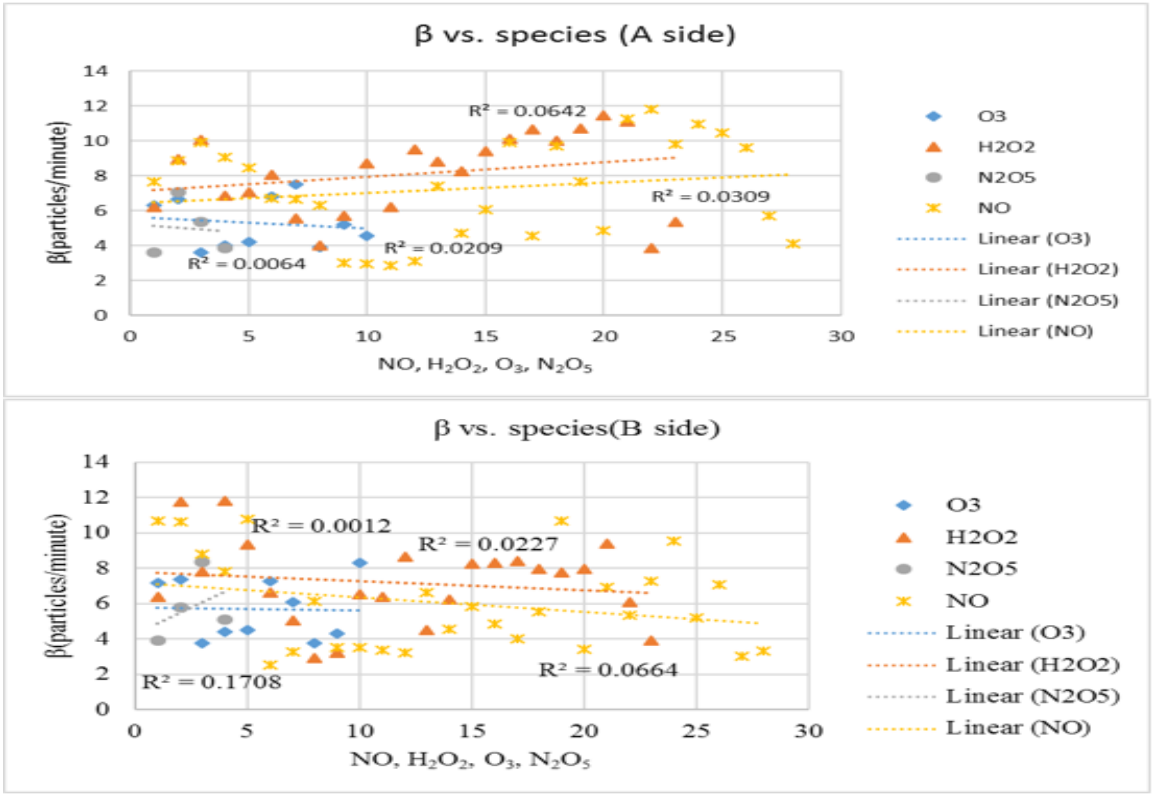

Figure (5). β vs. species (O_3, NO, N_2O_5, H_2O_2) from A side (top) and B side (bottom). No functional relationship between the wall loss rate, β, and either one of the compounds, NO, H_2O_2, O_3, and N_2O_5, is detected from the reactors in both sides. All the R^2's are less than 0.2.

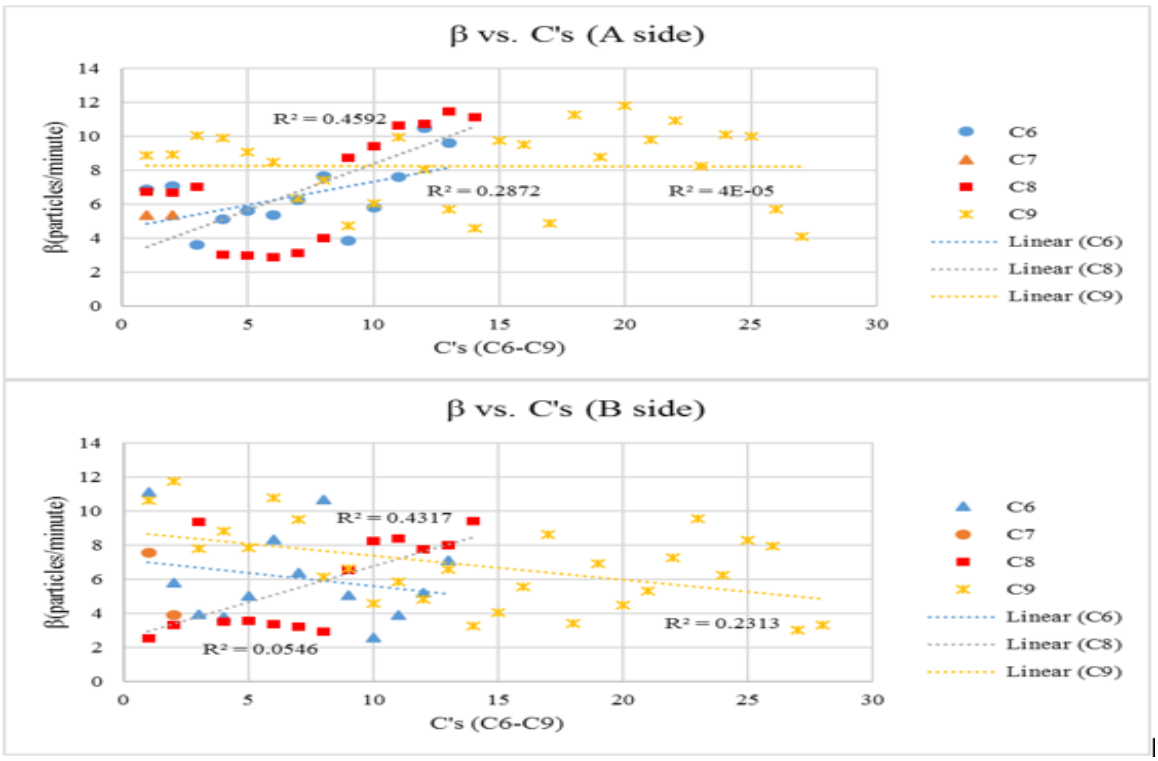

Figure (6). β vs. C's (C6-C9) from A side (top) and B side (bottom). A trend between the wall loss rate, β, and either one of the aromatic species from C6 to C9 is not observed from both sides of the reactors. All the R^2's are less than 0.5.

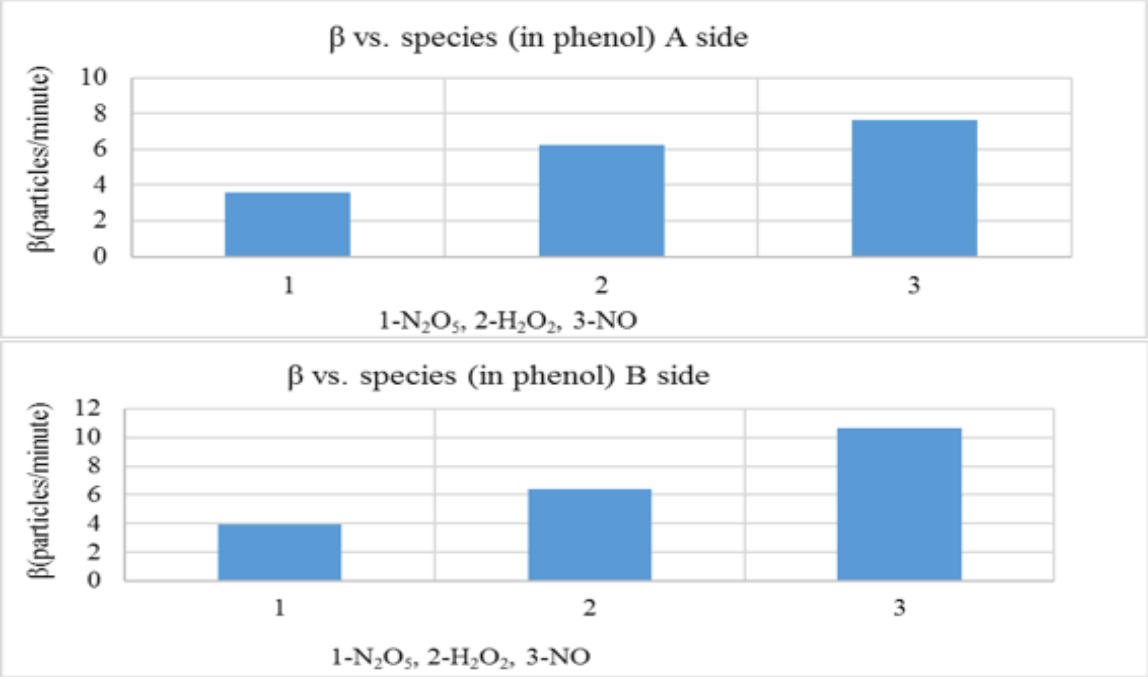

Figure (7) β vs. species (N_2O_5, H_2O_2, NO) from experiments EPA 1219, EPA 1217, and EPA 1184 from A side (top) and B side (bottom). The wall loss rate, β, increases as one of the reactants alters from N_2O_5, to H_2O_2, and finally to NO while keeping the other reactant, phenol, unchanged.

From Figures (1)-(6), it was observed that the wall loss rate, β, was independent (R^2<0.2) from the parameters (PM(num), M_o, T and MW), the non-carbon species (NO, H_2O_2, O_3, and N_2O_5), and the number of starting carbon in aromatic species from C6 to C9. In these figures, β showed no correlation with the parameters, the non-carbon species, and the aromatic species. A trend was not identified in any one of these figures. However, in Figure (7), β increased as one of the components altered from N_2O_5 to H_2O_2 and finally to NO while keeping the other component (phenol) unchanged. This trend implied the existence of a functional relationship between β and some of these parameter(s), PM(num), M_o, T, MW. Further investigation is needed to reveal more about this relationship in the future.

Figures (8)-(11) depicted particles loss to the walls. In these figures, all the PMNUMCOR curves reached their peak values at a time before their PMVOLCOR curves peaked. Thereafter, the PMNUMCOR curves declined while the corresponding PMVOLCOR curves were still increasing. This indicated that some of the particles in the chamber were lost to the walls, resulting in a decrease in PM number while the PM volume was still increasing. Figures (12)–(14) displayed the impact of the reactants' concentration on the PM formation. It was observed that by increasing the concentration of one of the reactants while keeping the concentrations of the other reactant unchanged, the PM formation increased accordingly. Figures (15)-(18) illustrated the effect of the molecular weight and size of compounds on the PM formation. In this comparison, the order of decrease in the molecular weight and size of the molecules under study is, N_2O_5 >H_2O_2 >NO. It was evident that by keeping the other component(s) unchanged, altering one of the components from H_2O_2 into NO produced more PM particles. Figure (17) also demonstrated that the addition of H_2O_2 decreased the number of PM compared with that in the chamber with NO but not H_2O_2. Figure (18) showed that with approximately the same concentration of phenol, changing N_2O_5 into H_2O_2 generated more PM. Figure (19) demonstrated that different isomers of xylenol had diverse effects on the PM formation. It was evident that 2,4-dimethylphenol was the most effective isomer in increasing the PM formation, whereas 3,5-dimethylphenol was the least effective among the isomers under study.

Conclusions

In this paper, the selected previous studies were reviewed. The general characterization of the environmental chamber, wall-loss, SOA formation and yields, and experimental approach were described. 100 sets of experimental results generated from the studies conducted at the UCR laboratory about the PM formation were reanalyzed. The relationships between β and each of the parameters (PM(num), M_o, T, and MW), the non-carbon species (NO, H_2O_2, O_3, and N_2O_5), and the number of starting carbon in aromatic species from C6 to C9; between the PM volume (both uncorrected and corrected) and t; and between PM number and t were reexamined. Based on the tables and graphs from the selected former studies as well as the graphs created from the UCR experimental results, the following conclusions were made. SOA deposited on the walls of environmental chamber, leading to the underestimation of SOA yields. No functional relationship between β and any one of the parameters (PM(num), M_o, T, and MW), the non-carbon species (NO, H_2O_2, O_3, and N_2O_5), the aromatic species from C6 to C9, and the chamber's volume (or surface area), was identified in the data under study. There were four major factors that affected the SOA formation. First, the effect of the SOA formation changed as the basic experimental conditions altered. These basic conditions included temperature, pressure, intensity of UV-visible light (irradiation), and relative humidity. Second, the defined experimental conditions based on the experimental objectives had impacts on the SOA formation. These conditions included the composition of the reactants such as the concentration of NO, O_3 and H_2O_2, the flow rates of the feeding gases, the effect of mass transfer, and the background of the chamber including seeded or seedless. Third, the chemical and physical properties of the reactants and reactor influenced the SOA

formation. The properties of the reactants affecting the SOA formation included the functional group(s) of the compound in the molecule, the compound's wall accommodation coefficient, $\alpha_{w,i,}$ the volatility of the compound, the charge of the particles formed from the compounds, and the particle size. The properties of the reactor that could alter the SOA formation were the activity coefficients in Teflon film and the ratio between the surface area and the volume of the chamber. Finally, the duration of the experiment also played a role in the amount of SOA formation.

Recommendations

To further study the relationships between β and each of the parameters (PM(num), M_o, T, and MW), the non-carbon species (NO, H_2O_2, O_3, and N_2O_5), and the number of starting carbon in aromatic species from C6 to C9, more runs of the corresponding experiments are recommended. Also, investigating the effect of extremely low volatility organic compounds (ELVOCs) on the SOA formation is recommended. It is known that ELVOCs have strong impacts on the SOA formation. However, measuring ELVOCs requires special instrumentation; besides, technical difficulties in measurement may occur. As a result, their impacts on the SOA formation need more investigation (Goldstein, Allen H., and John H. Seinfeld, 2015). The effects of the chamber wall materials on the wall-loss and SOA formation is another area that can be explored in future study as well.

Appendix

Graphs

1. Examples of SOA wall loss for representative chamber experiments.

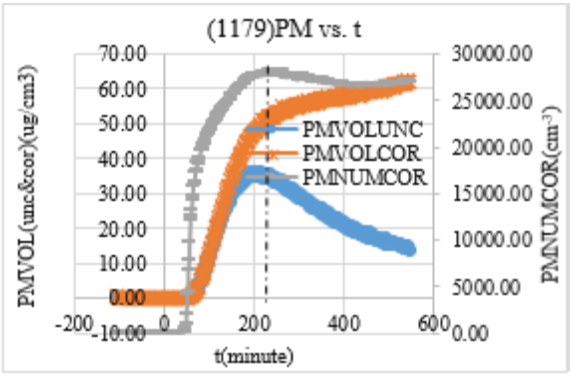

Figure(8). EPA1179-o-ethyltoluene 100ppb + NO 50ppb. The curve of PMNUMCOR reached the peak value of 66µg/cm^3 at 200 minute while the curve of PMVOLCOR was still rising.

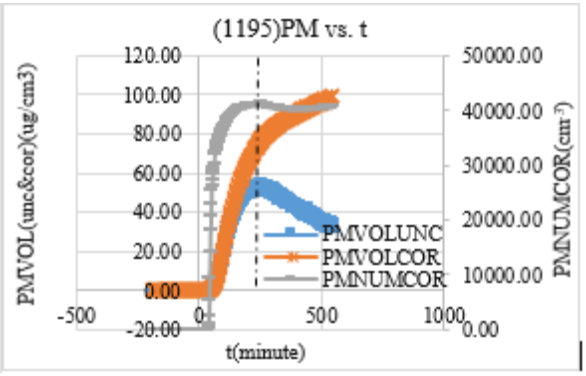

Figure (9). EPA 1195-benzene 1ppm +NO 50ppb +H_2O_2 200ppb. The curve of PMNUMCOR reached the peak value of 95µg/cm^3 at 230 minute before the curve of PMVOLCOR reached its peak value after 500 minutes.

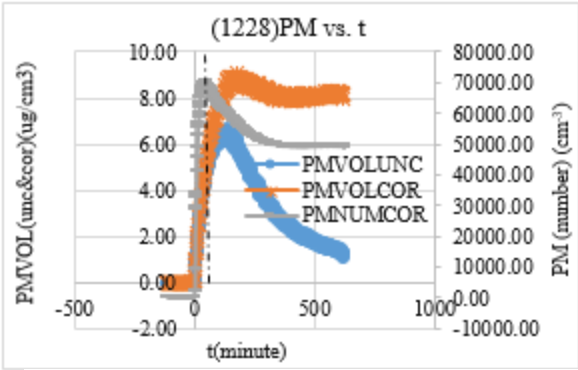

Figure (10). 1228- beta-caryophyllene 5ppb + O_3 150ppb + 2-butanol 1ppm. The PMNUMCOR curve reached its peak value, 9µg/cm^3, at 100 minute before the PMVOLCOR curve reached its peak value, 9.3µg/cm^3, at 200 minute.

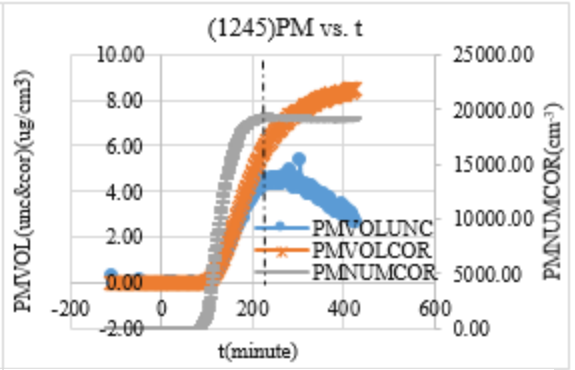

Figure (11). 1245-propylbenzene 0.1ppm + NO 20ppb. About 220 minutes after the light was on, the PM number reached its maximum when the PM corrected volume was still rising.

2. Examples about the impact of the reactant(s)' concentration(s) on PM formation

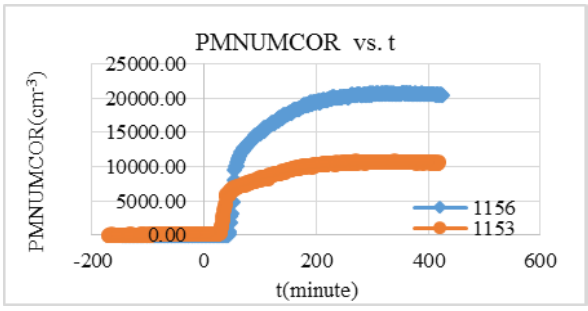

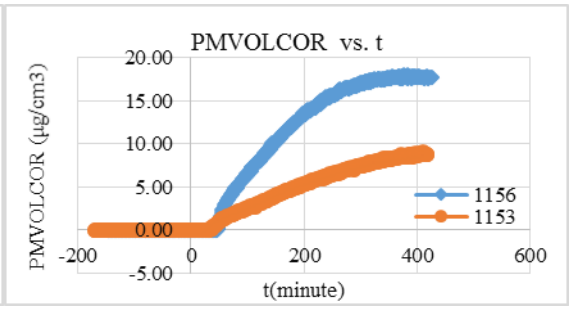

Figure(12). 1153- 1,3,5-Trimethylbenzene 80ppb + NO 10ppb; 1156- 1,3,5-trimethylbenzene 80ppb + NO 30ppb. The experiment of 1156 had more PM number in the chamber, especially at its maximum, 20,000 particle/cm^3, compared with 10,000 particles/cm^3 in the experiment of 1153. In addition, its PMVOLCOR curve had a steeper slope.

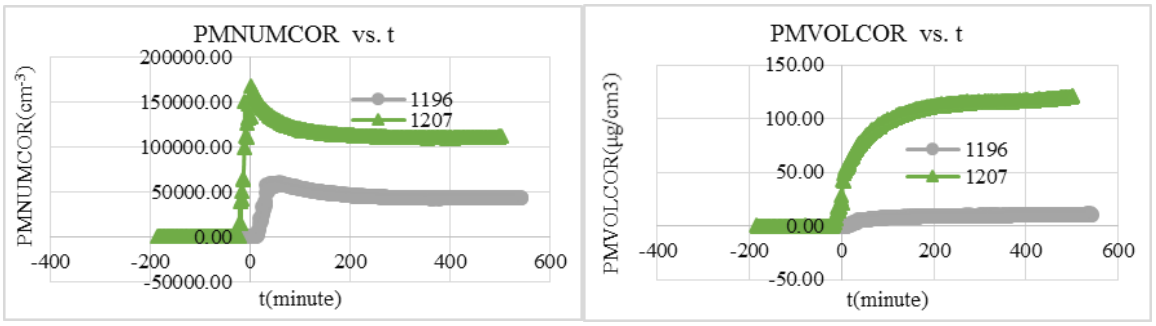

Figure (13). 1196- beta-caryophyllene 5ppb +O3 150ppb; 1207- beta-caryophyllene 20 ppb + O3 150ppb. The organic aerosols formed in the run of 1207 was detected before the light was on, whereas it was not until about 20 minutes after the light was on in the run of 1196. The PM number as well as the corrected volume in the run of 1207 were greater than those in the run of 1196 in the entire process.

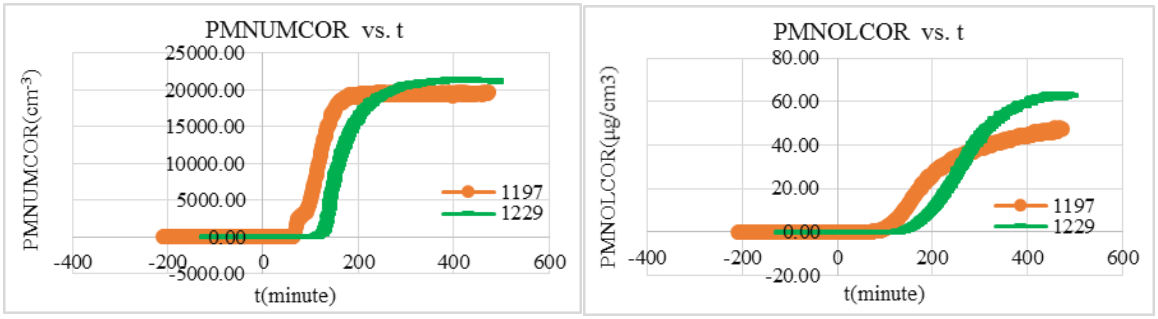

Figure (14). 1197- p-ethyltoluene 0.2ppm + NO 50ppb; 1229- p-ethlytoluene 0.2ppm + NO 150ppb. Compared with the experiment of 1197, the PM number and PM volume in the chamber of the experiment 1229 were greater during the test.

3. Examples about the effect of the molecular weight and size of compound on PM formation.

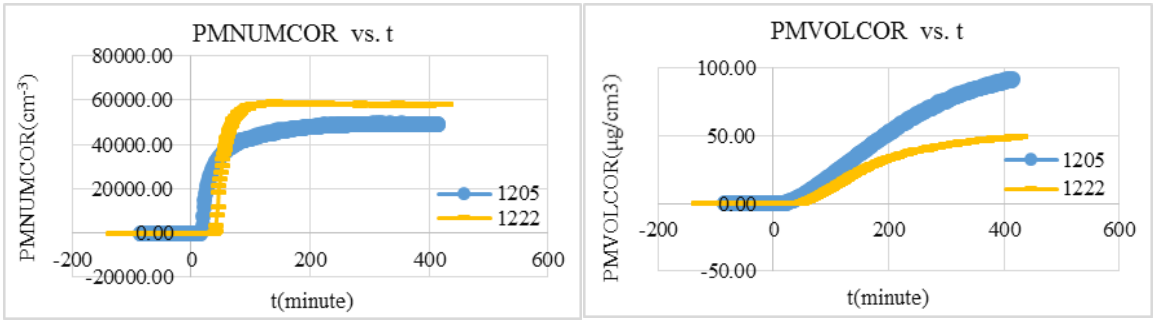

Figure(15). 1222- m-ethyltoluene 0.1ppm + NO 100ppb; 1205- m-ethyltoluene 0.1ppm + H2O2 1ppm. In the run of 1222, the PM number was greater whereas its PM volume was less compared with those in the run of 1205.

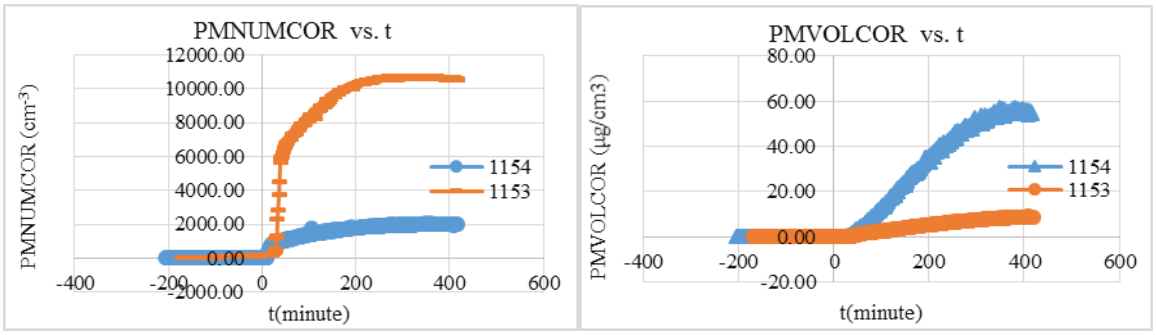

Figure (16). 1153- 1,3,5-Trimethylbenzene 80ppb + NO 10ppb; 1154- 1,3,5-trimethylbenzene 80 ppb+ H2O2 1ppm. Compared with the experiment of 1154, the PM number was significantly greater and its PM volume was remarkedly less than those in the experiment of 1153.

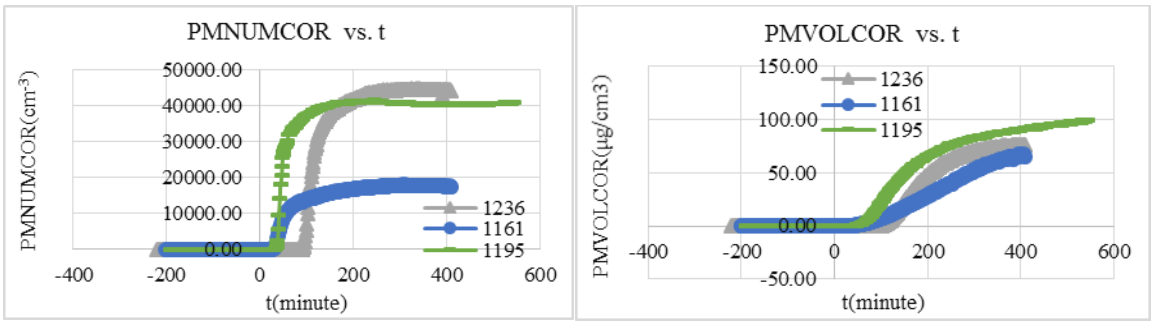

Figure (17). 1236- benzene 1ppm + NO 50ppb; 1161- benzene 1ppm + H2O2 5ppm; 1195- benzene 1ppm+ NO 50ppb + H2O2 200ppb. Among these three experiments, the experiment of 1236 had the latest detectable but greatest peak value in the PM number. Its PM volume was a size between that in the experiment of 1195 and that in the experiment of 1161. The least PM number was observed in the experiment of 1161 with the smallest size in the PM volume.

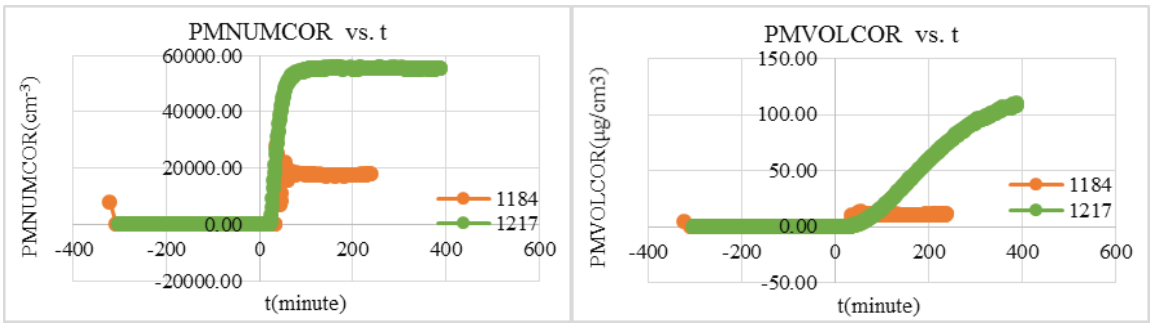

Figure (18). 1184- phenol 123ppb + N2O5 130ppb; 1217- phenol 120ppb + H2O2 2ppm. The run of 1217 was greater either in the PM number or in the PM volume in the chamber compared with the run of 1184.

4. Examples about the impact of the position(s) of functional group(s) in an isomer on the effect of PM formation

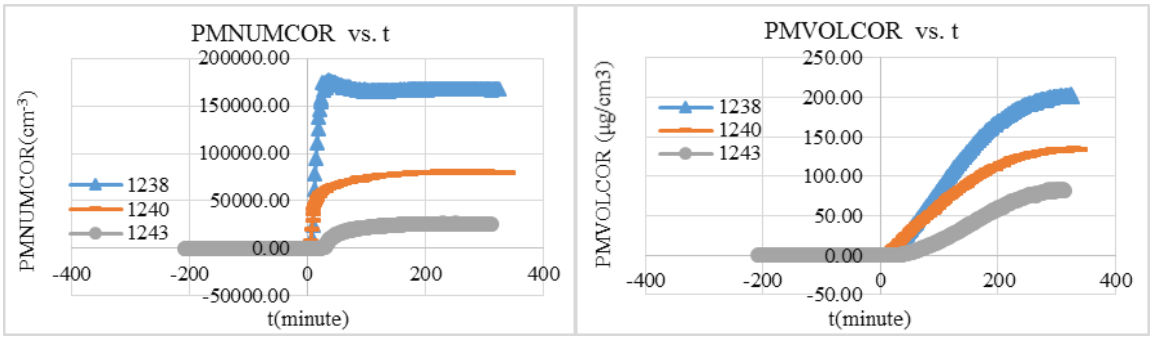

Figure (19). 1238- 2,4-dimethylphenol 80ppb + H2O2 1ppm; 1240- 2,6-dimethylphenol 80ppb + H2O2 1ppm; 1243- 3,5-dimethylphenol 80ppb + H2O2 1ppm. Among the three experiments, the experiment of 1238 had the greatest PM number and PM volume detected in the chamber, whereas the experiment of 1243 had the least in both.

References

1. Bian, Q., A. A. May, S. M. Kreidenweis, and J. R. Pierce. "Investigation of Particle and Vapor Wall-loss Effects on Controlled Wood-smoke Smog-chamber Experiments." *Atmospheric Chemistry and Physics* (2015): n. pag. 5 June 2015. Web. 15 June 2016.
2. Carter, William P. L, David R. Cocker III, Dennis R. Fitz, Irina L. Malkina, Kurt Bumiller, Claudia G. Sauer, John T. Pisano, Charles Bufalino, and Chen Song, "A New Environmental Chamber for Evaluation of Gas-phase Chemical Mechanisms and Secondary Aerosol Formation." *Atmospheric Environment*, 15 Aug. 2005. Web. 16 June 2016.
3. Cao, G, and Jang, M. "Secondary organic aerosol formation from toluene photooxidation under various NOx conditions and particles acidity." *Atomospheric Chemistry and Physics Discussion*, 30 July 2008. Web. 15 June 2016.
4. Carter, William P.L, Gookyoung Heo, David R. Cocker III, and Shunsuke Nakao. "SOA FORMATION: CHAMBER STUDY AND MODEL DEVELOPMENT." *Arby's.CA*. California Air Resources Board, 29 Mar. 2012. Web. 15 June 2016.
5. Goldstein, Allen H., and John H. Seinfeld. *Effect of Vapor Wall Loss in Laboratory Chambers on Yields of Secondary Organic Aerosols*. Pasadena: California Institute of Technology, 2015. California Air Resouce Board, Sept. 2015. Web. 16 June 2016.
6. Kulkarni, Pramod, Paul A. Baron, and Klaus Willeke. "Aerosol Measurement: Principles, Techniques, and Applications." *Google Books*. JOHN WILEY &SONS. INC, 2011. Web. 15 June 2016.
7. La, Y. S., M. Camredon, P. J. Ziemann, R. Valorso, A. Matsunaga, V. Lannuque, J. Lee-Taylor, A. Hodzic, S. Madronich, and B. Aumont, "Impact of Chamber Wall Loss of Gaseous Organic Compounds on Secondary Organic Aerosol Formation: Explicit Modeling of SOA Formation from Alkane and Alkene Oxidation." *Atmospheric Chemistry and Physics* (2016): n. pag. Atmospheric Chemistry and Physics, 8 Feb. 2016. Web. 16 June 2016.
8. Leskinen, A, P. Yli-Pirila, K. Kuuspalo, O. Sippula, P. Jalava, M. -R. HIRVONEN, J. Jokiniemi, A. Virtanen, M. Komppula, and K. E. J. Lehtinen, "Characterization and Testing of a New Environmental Chamber Designed for Emission Aging Studies." *ResearchGate*. Atmospheric Measurement Techniques, 3 June 2015. Web. 16 June 2016.
9. Matsunaga, Aiko, and Paul J. Ziemann. "Gas-Wall Partitioning of Organic Compounds in a Teflon Film Chamber and Potential Effects on Reaction Product and Aerosol Yield Measurements." *Taylor & Francis*. Aerosol Science and Technology, 10 Aug. 2010. Web. 16 June 2016.
10. Pierce, J. R., G. J. Engelhart, L. Hildebrandt, E. A. Weitkamp, R. K. Pathak, N. M. Donahue, A. L. Robinson, P. J. Adams, and S. N. Pandis, "Constraining Particle Evolution from Wall Losses, Coagulation, and Condensation-Evaporation in Smog-Chamber Experiments: Optimal Estimation Based on Size Distribution Measurements." *Aerosol Science and Technology*, 26 Sept. 2008. Web. 16 June 2016.
11. Wang, X, T. Liu, F. Bernard, X. Ding, S. Wen, Y. Zhang, Z. Zhang, Q. He, S. Lu, J. Chen, S Sannders, and J. Yu, "Design and Characterization of a Smog Chamber for Studying Gas-phase Chemical Mechanisms and Aerosol Formation." *Atmospheric Measurement Techniques*, 29 Jan. 2014. Web. 16 June 2016.
12. Zhang, Xuan, Christopher D. Cappa, Shantanu H. Jathar, Renee C. McVay, Joseph J. Ensberg, Michael J. Kleeman, and John H. Seinfeld, "Influence of Vapor Wall Loss in Laboratory Chambers on Yields of Secondary Organic Aerosol." *Pans.org*. John. H. Seinfeld, 12 Mar. 2014. Web. 15 June 2016.